

WIDEBAND PLANAR SLOT ANTENNAS

Abdelnasser A. Eldek, Atef Z. Elsherbeni, Charles E. Smith and Kai-Fong Lee

Center of Applied Electromagnetic Systems Research (CAESR)
Department of Electrical Engineering, The University of Mississippi, University, MS 38677

Abstract — In this paper a printed dipole antenna and three slot antennas are designed to operate at 10 GHz for use in radar systems. A parametric study of each antenna and comparison between their radiation properties including return loss, bandwidth, directivity, efficiency and radiation patterns for 6-element linear array are introduced. Slot antennas show wider bandwidth, less coupling and smaller antenna size compared with the microstrip printed dipole.

I. INTRODUCTION

In present-day radar systems, the need for antennas of small size and high efficiency has generated much attention in the study of compact microstrip antennas. These antennas exhibit low profile and lightweight properties as well as low cross polarization radiation in some designs. However, microstrip antennas inherently have narrow bandwidths (BW) and in general are half-wavelength structures operating at the fundamental resonant mode [1]. The coplanar patch antennas (CPAs) introduced in [2] and [3] have 3.4% and 8.8% BW, respectively. Researchers have made efforts to overcome the problem of narrow BW and various configurations have been presented to extend the BW. Adding a short on the upper slot of the CPA and varying its length achieved 30 to 40% BW [4] at higher frequencies for radar applications. A number of bow-tie slot designs are recently introduced, which demonstrate wide bandwidth that ranges from 17% to 40% [5-10].

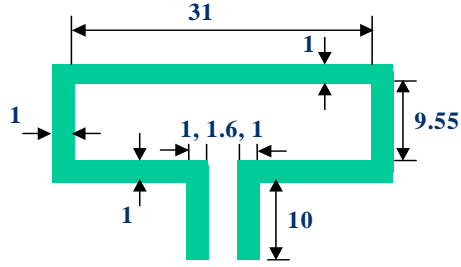
In this paper, printed dipole, coplanar patch-slot (CPA), slot dipole and bow-tie slot antennas have been designed for radar applications with emphasis on size reduction, and improved BW, coupling and efficiency for antenna arrays. Characteristics of arrays of 6 elements of these antennas are compared with the printed dipole design, and their S-parameters and radiation properties are introduced.

II. ANTENNA ANALYSIS

The numerical analysis of the antennas studied is performed using the commercial computer software package, Momentum of Agilent Technologies, Advanced Design System (ADS), which is based on the method of moment (MoM) technique for layered media. Momentum solves mixed potential integral equations (MPIE) using full wave Green's functions. First, a comparison of the results of ADS with measured results of a CPA presented in [2] reveals good agreement, as shown in Fig. 1, and this gives credibility to the results of the ADS simulation. Another verification for the results of ADS is confirmed by a comparison with the results from a simulation based on the finite difference time domain (FDTD) technique.

A. Printed Dipole Antenna

The geometry of a printed dipole and its parameters are shown in Fig. 2, where W represents the dipole width, L_f is the feed line length, $t1$ is the dipole height, $t2$ is the feed line width and G is the gap width. In addition to these parameters, h is the height of the substrate, and ϵ_r is the dielectric constant.



Substrate with backed ground plane, where $\epsilon_r = 2.17$ and $h = 0.508$ (height). All dimensions are in mm.

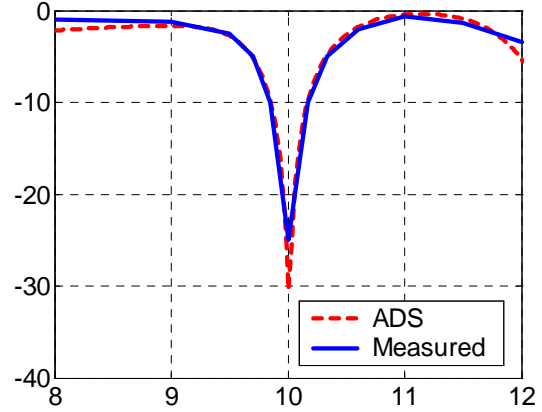


Fig. 1. Verification with measured results of the CPA presented in [2].

The return loss of the printed dipole based on ADS Momentum is confirmed by comparing the numerical results from a FDTD computation. This comparison reveals good agreement, as shown in Fig. 3. The presented printed dipole has $(W, t1, t2, G, l_f \text{ and } h) = (12.4, 0.5, 0.3, 0.4, 0.3 \text{ and } 1.57 \text{ mm})$ and $(\epsilon_r = 2.2)$.

The parametric study of this structure starts with the feed line length L_f . By increasing L_f , it is noticed that the resonant frequency decreases, then increases back towards the original frequency at certain length. It is known that the input impedance for a transmission line is given by

$$Z_m = Z_0 \frac{Z_L + jZ_0 \tan \beta l}{Z_0 + jZ_L \tan \beta l}. \quad (1)$$

At $l = \lambda g/2$, $Z_m = Z_L$, and, from this, a numerical experiment can be performed to define λg of this antenna. Then, the effective permittivity, ϵ_{eff} , can be calculated from

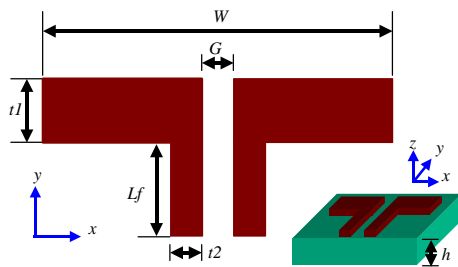


Fig. 2. Printed dipole antenna parameters.

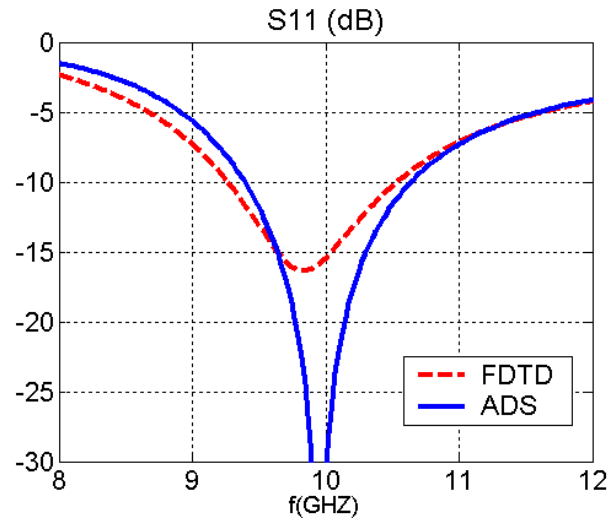


Fig. 3. ADS Momentum and FDTD results for the printed dipole antenna.

$$\lambda_g = \frac{\lambda_0}{\sqrt{\epsilon_{reff}}} . \quad (2)$$

The λ_g of this printed dipole is 23 mm and ϵ_{reff} is about 1.7, which is 77% of ϵ_r . LineCalc, a program within the ADS software package, calculates ϵ_{reff} of the two strip feed line to be 1.78 which shows that the printed dipole antenna structure decreases the feed line ϵ_{reff} . Additional parametric study for this antenna shows that increasing W , h and ϵ_r reduces the resonant frequency, and that t/l and the feed line parameters control the return loss level. Further study shows that the dominant factor in the design of printed dipoles is W , which traditionally assumed to be $\lambda_g/2$. This antenna has more than 12 % BW and 90 % efficiency.

B. Slot Dipole Antenna

The slot dipole geometry and its parameters are shown in Fig. 4, where W represents the dipole width, SI is the slot height, L_{cpw} is the length of the coplanar waveguide (CPW) feed line, and $S2$ and G are the width and gap width of the CPW. In addition to these parameters, h is the height of the substrate, and ϵ_r is the dielectric constant.

The slot dipole presented in this paper has for the following parameters, W , SI , L_{cpw} , $S2$, G and h , the values 19.3, 1.5, 1.5, 0.25, 1, and 1.57 mm and $\epsilon_r = 2.2$. Figure 5 shows a comparison between ADS Momentum and FDTD results for the presented slot dipole. This comparison reveals good agreement and confirms our design procedure using Momentum.

L_{cpw} behaves like L_f in the printed dipole, and λ_g and ϵ_{reff} are calculated by the same procedure used previously. The calculated λ_g of the slot dipole is found to be 23.5 mm and $\epsilon_{reff} = 1.63$ (74% of ϵ_r), respectively. The ϵ_{reff} of the CPW feed line based on LineCalc calculations is 1.576, which shows that the slot dipole antenna structure increases the feed line ϵ_{reff} . By observing the influence of various parameters on the antenna performance, it is found that increasing W , SI , h and ϵ_r decreases the resonant frequency, and SI and the feed line parameters control the return loss level. Further study shows that the total slot length, calculated at the centerline of the slot, is about λ_g and W is about $0.82 \lambda_g$. This antenna can provide more that 21 % BW and 80 % efficiency.

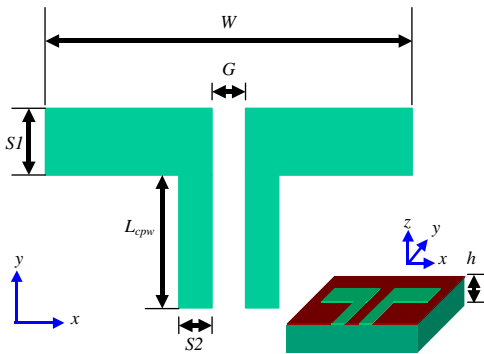


Fig. 4. Slot dipole geometry and parameters.

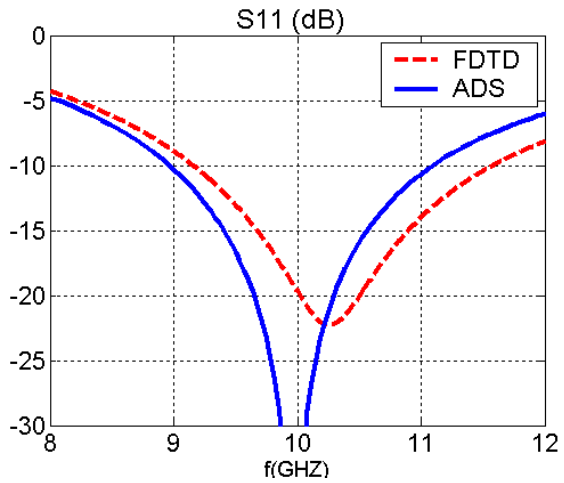


Fig. 5. ADS Momentum and FDTD results for the slot dipole antenna.

C. Coplanar Patch-Slot Antenna

The geometry of the CPA and its parameters are shown in Fig. 6. The antenna consists of a rectangular patch surrounded by a non-uniform width slot. As shown in Fig. 6, W represents the patch width, L is the patch length, and $S1$, $S2$ and $S3$ are the widths of the upper slot, left-right slot, and lower slot, respectively. $S4$ and $S5$ are the gap width and feed line width of the CPW, and L_{cpw} represents the length of the CPW. In addition to these parameters, h is the height of the substrate, and ϵ_r is the dielectric constant.

The dimensions of the CPA presented in this paper and the antenna of [2] are shown in Table 1. The presented CPA does not have conductor-backed ground plane while the CPA of [2] has one. A comparison between these two antennas shows an improvement in BW from 3.4 % to 17 %, as shown in Fig. 7. Furthermore, the presented CPA is 60 % less in width than that of [3]. Figure 8 shows a comparison between ADS and FDTD results for the presented CPA. This comparison reveals good agreement.

For this antenna, L_{cpw} also behaves like L_f in the printed dipole antenna design, and λ_g and ϵ_{reff} are calculated, using the same procedure used for the dipole, to be 23.5mm and 1.54 (70 % ϵ_r), respectively. LineCalc calculation of ϵ_{reff} of the CPW feed line is 1.58, which shows that the CPA antenna decreases the feed line ϵ_{reff} . By observing the influence of various parameters on the antenna performance, it is found that increasing W , L , h , ϵ_r , $S1$ and $S2$ and decreasing $S3$ reduce the resonant frequency. The CPW feed line parameters control the return loss level. Although the effect of all these parameters is clear on f_c , it is not clear which one parameter can primarily increase the BW of the antenna. In CPA design, the dominant factors are W , L and the total slot length (L_{total}), calculated at the centerline of the slot, where

$$L_{total} = 2(W+L+L_{cpw}+S2+S3)+S1-S4-S5. \quad (3)$$

By studying the given design at various center frequencies, it is clear that W is about $0.5\lambda_g$, and the L_{total} is about $1.5\lambda_g$. At the same time L is about $0.1\lambda_g$. In general, L_{total} controls the resonant frequency while patch dimensions and slot widths control the level of return loss and the resulting BW. Our study revealed that this antenna yields more than 17 % BW and 80 % efficiency.

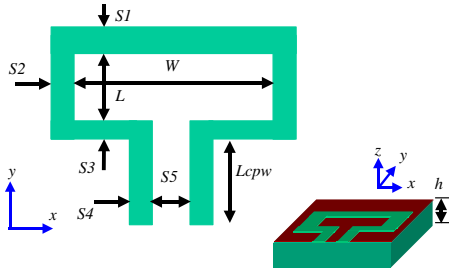


Fig. 6. CPA geometry and parameters.

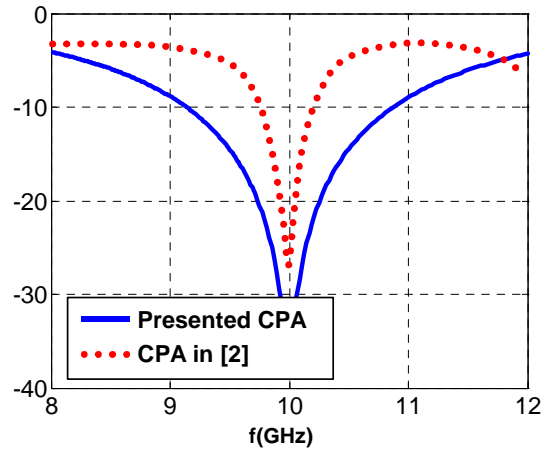


Fig. 7. Return loss comparison between the presented CPA and that of [3].

Table 1. Dimensions in mm of the CPA of [2] and the presented CPA antenna working at 10 GHz.

	W	L	L_{cpw}	$S1:S5$	h	ϵ_r
CPA of [2]	31	9.55	10	1, 1, 1, 1, 1.6	0.508	2.17
Presented CPA	12.4	2.0	1.5	0.5, 0.25, 0.5, 0.25, 0.75	1.57	2.2

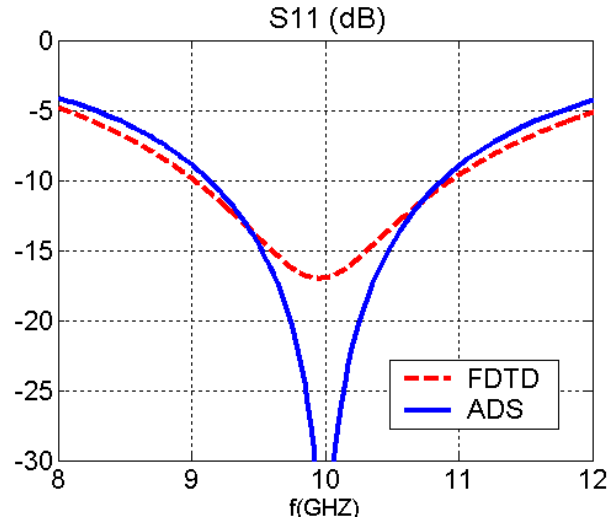


Fig. 8. Comparison between the ADS Momentum and FDTD results for the presented CPA.

D. Bow-Tie Slot Antenna

The geometry of the bow-tie slot antenna and its parameters are shown in Fig. 9, where W_1 represents the width, L_{cpw} is the feed line length, L_1, L_2, L_3, L_4 and W_2 define the bow shape, and S_1 and S_2 define the feed line parameters. In addition to these parameters, h is the height of the substrate, and ϵ_r is the dielectric constant. The presented bow-tie design has the parameters $W_1, W_2, L_1, L_2, L_3, L_4, L_{cpw}, S_1, S_2$, and h being set equal to 22.9, 8.7, 3.5, 20.75, 19.45, 7.35, 18.5, 0.25, 3, and 1.57 mm, respectively, and $\epsilon_r=2.2$. Figure 10 shows a comparison between ADS Momentum and FDTD results for the presented bow-tie slot antenna. Although a stair case geometry is used in FDTD approach to define the bow-tie geometry, and only one cell is used in the feed line slot due to memory restrictions, the comparison reveals acceptable agreement, which confirms our design procedure using Momentum.

It is found that L_{cpw} behaves similar to L_f as in the printed dipole, and λ_g , and ϵ_{reff} are calculated to be 22.5 mm and 1.78 (80 % ϵ_r), respectively, using the same procedure. LineCalc calculates ϵ_{reff} of the bow-tie slot feed line to be 1.51, which shows that the bow-tie clearly increases the feed line ϵ_{reff} . By observing the influence of various parameters on the antenna performance, it is found that resonant frequency decreases when increasing h, ϵ_r, W, L_2 and L_4 , and, when decreasing W_2, L_1, L_3 and S_1 and increasing S_1, L_1 and L_3 , increases the BW. It is also determined that the feed line dimensions control the return loss level at the center frequency. By studying the given design at various center frequencies, it is clear that W is about λ_g and the L_4 is about $0.3\lambda_g$. This antenna can yield more than 40 % BW and 80 % efficiency.

The bow-tie slot antenna is fabricated and the return loss is measured using the HP 8510C vector network analyzer (VNA). The fabricated antenna has a finite ground plane truncated at 1 cm away from the bow-tie slot edge. Figure 11 shows the antenna and the coaxial connector used to feed it. The antenna with finite ground plane is simulated using ADS Momentum and Fig. 12 presents the measured and simulated results, which reveals a good agreement. The measured return loss for the finite ground plane bow-tie slot antenna has a bandwidth of 52%, which is better than the simulation results.

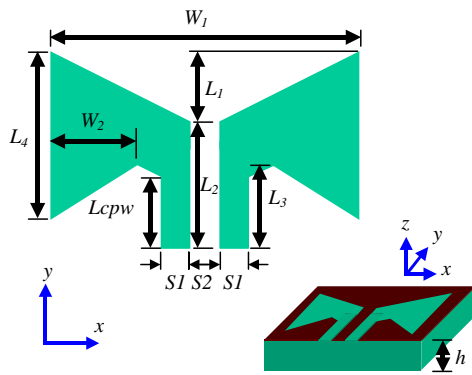


Fig. 9. Bow-tie slot antenna geometry and parameters.

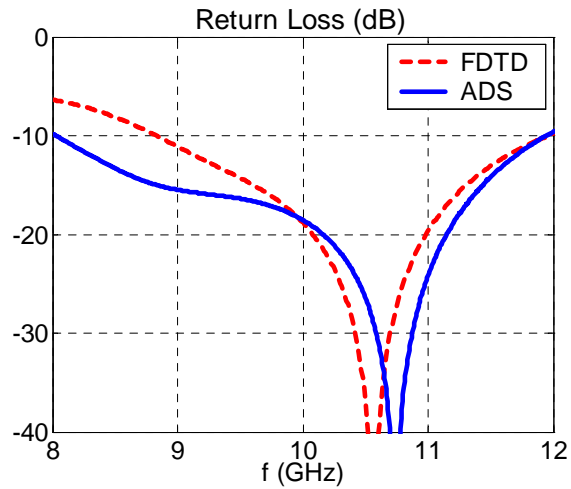


Fig. 10. Comparison between the ADS Momentum and FDTD results for the presented Bow-tie slot antenna.

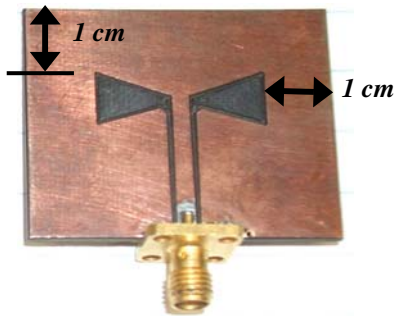


Fig. 11. The finite ground plane bow-tie slot antenna used in measurement.

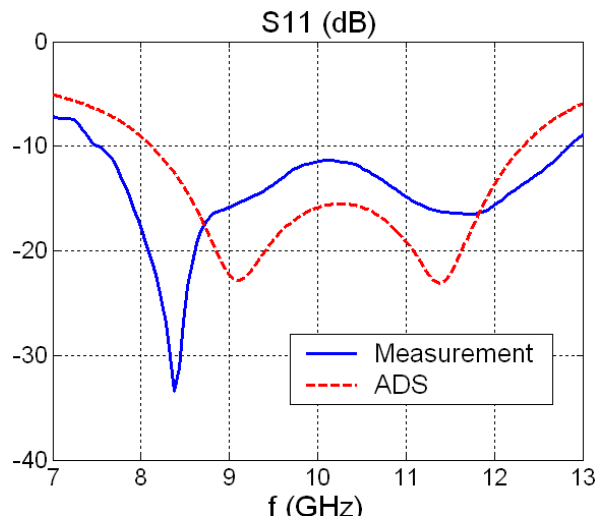


Fig. 12. Measured and ADS Momentum results of the finite ground plane bow-tie slot antenna.

III. SINGLE ELEMENT CHARACTERISTICS

Figures 3, 5, 8 and 10 show that the *BW* of the printed dipole antenna, the CPA, the slot dipole and the bow-tie are 12.5 %, 17 %, 21 % and 40 %, respectively. The stability of the radiation properties of each antenna, as a single element, in the operating band has been investigated. Table 2 shows the stability characteristic of each antenna by showing directivity (*D*), gain (*G*) and efficiency (η) at selected frequencies covering the entire operating band. In general, all the antennas show good stability over the entire band. The radiation patterns of the presented antennas are shown in Figures 13, 14 and 15 in *x-y*, *x-z* and *y-z* plane, respectively. The printed dipole has no radiation in *x-y* plane, while the slot antennas radiate in *x-y* as shown in Fig. 13. In the *x-z* plane, the cross polarization level of the printed dipole antenna is less than -40 dB, the slot dipole -32 dB, the bow-tie -27 dB and the CPA -17 dB. In the *y-z* plane, the cross polarization level is 40 dB, which is why E_θ is not shown for the printed dipole and E_ϕ is not shown for the slot antennas. Antenna polarization and its relation with the radiation pattern are discussed in the next section for each antenna.

Table 2. Properties of the 4 presented antennas (single element) at selected frequencies covering the entire band.

Printed dipole			
<i>Freq. (GHz)</i>	<i>D (dB)</i>	<i>G (dB)</i>	$\% \eta$
9.40	3.05	2.03	79.07
9.80	3.12	1.99	77.09
10.2	3.19	1.96	75.34
10.6	3.27	1.92	73.28
Slot Dipole			
<i>Freq. (GHz)</i>	<i>D (dB)</i>	<i>G (dB)</i>	$\% \eta$
9.00	3.11	2.20	81.10
9.70	3.34	2.36	79.80
10.5	3.58	2.55	78.89
11.2	3.85	2.78	78.16
CPA			
<i>Freq. (GHz)</i>	<i>D (dB)</i>	<i>G (dB)</i>	$\% \eta$
9.10	2.84	2.00	82.41
9.70	2.93	2.03	81.28
10.3	3.02	2.07	80.35
10.9	3.10	2.10	79.43
Bow-Tie			
<i>Freq. (GHz)</i>	<i>D (dB)</i>	<i>G (dB)</i>	$\% \eta$
8.00	3.01	2.38	86.50
9.00	3.61	2.86	84.14
10.67	4.27	3.40	81.85
12.00	4.94	4.06	81.66

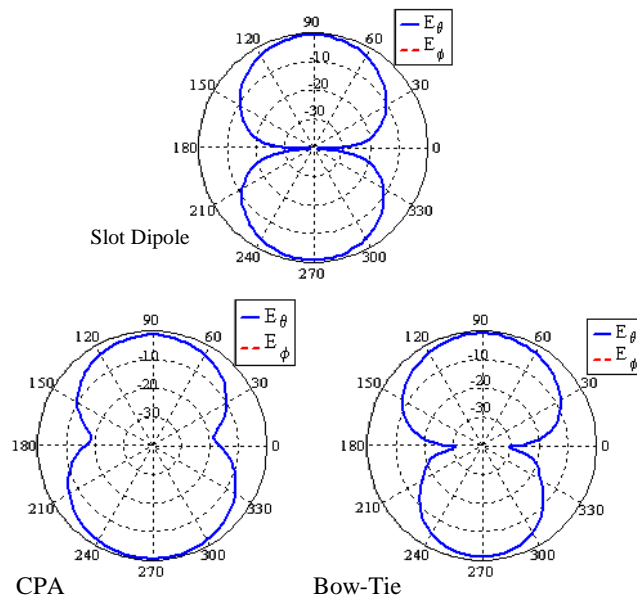


Fig. 13. Radiation pattern for single element in x-y plane.

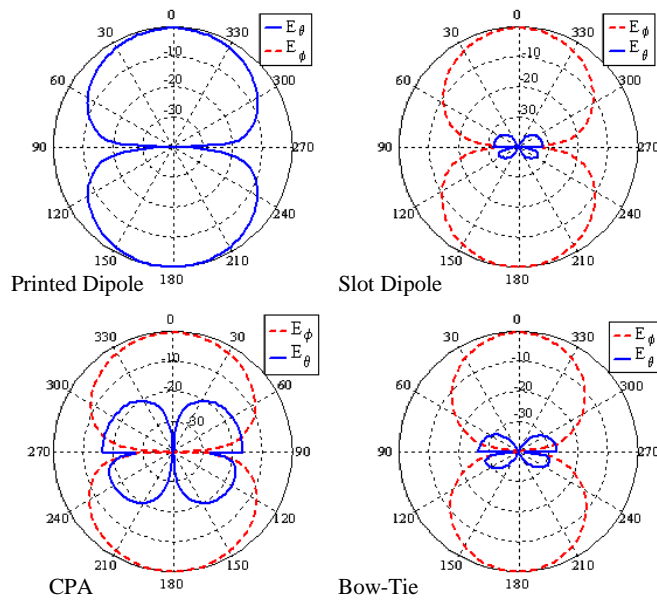


Fig. 14. Radiation pattern for single element in x-z.

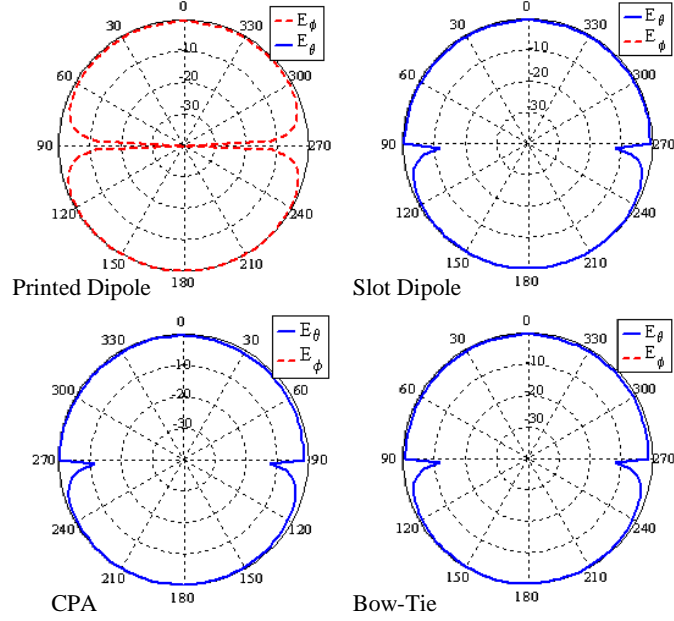


Fig. 15. Radiation pattern for single element in y - z planes.

A. Printed Dipole Antenna

The printed dipole is x -polarized because the electric current flows in x -direction as shown in Fig. 16. According to the antenna polarization and boundary conditions, the well known dipole-type radiation pattern can be expected. In the x - y plane, E_θ is normal to the direction of the polarization therefore it is zero. However E_ϕ is in the direction of the polarization at $\phi = \pi/2$, thereby it has a maximum there, but this maximum is less than 40 dB for this antenna. In the x - z plane, E_θ is in the direction of polarization at $\theta = \pi/2$, therefore it has a maximum at this angle, and it is zero at $\theta = 0$ because it is normal to the polarization direction, as shown in Fig. 14. At the same plane, x - z , E_ϕ is normal to the direction of polarization, therefore it is zero, as shown in Fig. 14. In the y - z plane, E_θ is normal to the direction of polarization, therefore it is also zero as shown in Fig. 15. At the same plane, y - z , E_ϕ is always in the direction of polarization, thus it should be uniform in this plane; however, because E_ϕ is tangential to the conductor at $\theta = \pi/2$, it goes to zero there, as shown in Fig. 15.

B. Slot Antennas

The slot antennas are y -polarized because, as shown in Figures 17, 18 and 19, the electrical fields tend to add in the y -direction and cancel each other in x -direction. According to the related antenna polarization and boundary conditions, a complementary slot-dipole type radiation pattern is obtained. In the x - y plane, E_θ is normal to the conductor, but because the antennas are y -polarized, E_θ has a maximum only in the y -direction, as shown in Fig. 13. In the x - y plane, E_ϕ must be zero because it is tangential to the conductor, as shown in Fig. 13. In the x - z plane, E_θ is normal to antenna polarization; therefore, it is expected to go to zero. But because E_θ is normal to the conductor at $\theta = \pi/2$, it has its maximum value there; however, this maximum is affected by the surface waves on the conductor and the dielectric, as shown in Fig. 14, where E_θ is zero at $\theta = 0$, and it has a maximum at $\theta = \pi/2$. This E_θ maximum in the x - z plane is larger for the CPA and smaller in the slot dipole. At the same plane, x - z , E_ϕ is in the direction of polarization, therefore it is

the co-polarized component, and, at $\theta = \pi/2$, it is zero because it is tangential to the conductor, as shown in Fig. 14. In the y - z plane, E_θ is in the direction of polarization at $\theta = 0$ and normal to the conductor at $\theta = \pi/2$; therefore, it has a uniform amplitude in this plane, but this uniformity is affected by the surface waves on the conductor and the dielectric at $\theta = \pi/2$, as shown in Fig. 15. At the same y - z plane, E_ϕ is always normal to the polarization direction and therefore it goes to zero, and that is shown in Fig. 15.

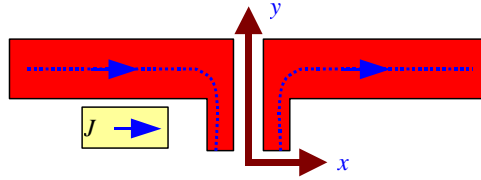


Fig. 16. Polarization in printed dipole.

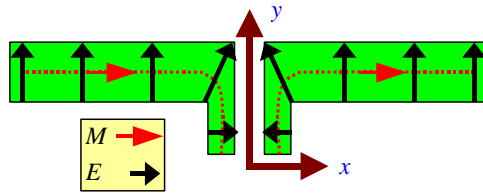


Fig. 17. Polarization in slot dipole.

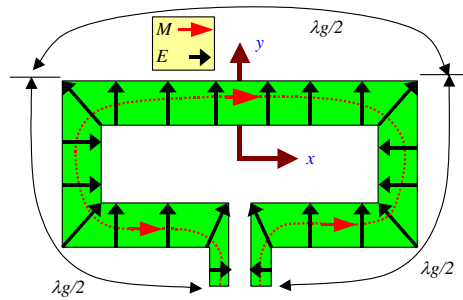


Fig. 18. Polarization in CPA.

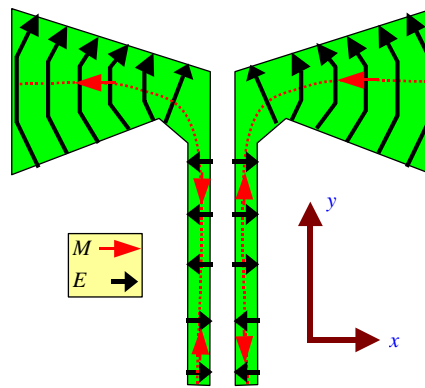


Fig. 19. Polarization in bow-tie slot antenna.

IV. ANTENNA ARRAY CHARACTERISTICS

A. Return Loss and Coupling

Arrays of the presented microstrip slot antennas, the slot dipole, the CPA and the bow-tie slot, along with the printed dipole antenna are designed. A comparison between 6-element array modules of these antennas is performed for operation at 10 GHz. For the 6-element array module, the distance between elements is chosen to provide a -24 dB magnitude for S_{21} (coupling between two neighboring elements). This distance is found to be 20.8 mm for the printed dipole, 4 mm for the slot dipole, 8.5 mm for the CPA and 4 mm for the bow-tie slot antenna, which indicates that the slot dipole and the bow-tie have the lower coupling and the printed dipole has the highest coupling for the same distance between elements. The return loss and coupling between elements for all designs are shown in Fig. 20. The bow-tie has 40 % BW, the slot dipole 21.5 %, and the CPA 17 %. The bow-tie has the lowest coupling levels between the first element and the other five elements; and the slot dipole and the CPA have the next lowest couplings.

B. Radiation Properties

Table 3 lists the BW, D , η and size reduction for the 6-element array of the slot antennas compared with that of the printed dipole. The directivity is approximately 11 dB, and the efficiency is 91.39 % for the printed dipole, 83.25 % for the CPA, 82.49 % for the slot dipole and 81.78 % for the bow-tie. The slot antenna arrays achieve size reduction relative to the printed dipole array ranging from 12 % for the bow-tie, 24 % for the slot dipole and 28 % for the CPA. The size reduction is based on the total length of the 6-element array relative to that of the printed dipole array. The total length is calculated as $[6 \times W_a + 5 \times d_s]$, where W_a is the width of the antennas, which equals to W for all antennas except the CPA. For the CPA, this length is $W + 2 \times S_2$, and d_s is the separation distance between the antennas.

Radiation patterns are calculated for 6-element array. The radiation pattern in x - y plane is shown in Fig. 21 for the slot antennas, while there is no radiation in the x - y plane by the printed dipoles. The co-polar and cross-polar radiation patterns in x - z and y - z planes are shown in Figs. 22 and 23, respectively. As shown in the x - z plane, the cross-polarization is less than -40 dB in the printed and slot dipole, -34 dB in the CPA, and -27 dB in the bow-tie where E_θ is the co-polar component in the printed dipole and E_ϕ is the co-polar in the slot dipoles. As shown in y - z plane, the cross-polar level is less than -40 dB for all antennas where E_ϕ is the co-polar component in the printed dipoles and E_θ is the co-polar in the slot antennas. Figure 24 shows the 3-dimension radiation pattern for all antennas. It is clear that the side lobe levels are higher in the printed dipole relative to those patterns of the slot antennas, which is not a desirable characteristic for phased antenna array system.

Table 3. Radiation properties for 6-element array.

	<i>BW (%)</i>	<i>D (dB)</i>	<i>η (%)</i>	<i>Reduction</i>
Printed dipole	12.5 %	11.28	91.39	0 %
Slot dipole	21.5 %	10.45	82.49	24 %
CPA	17.0 %	10.33	83.25	28 %
Bow-tie	40.0 %	10.65	81.78	12 %

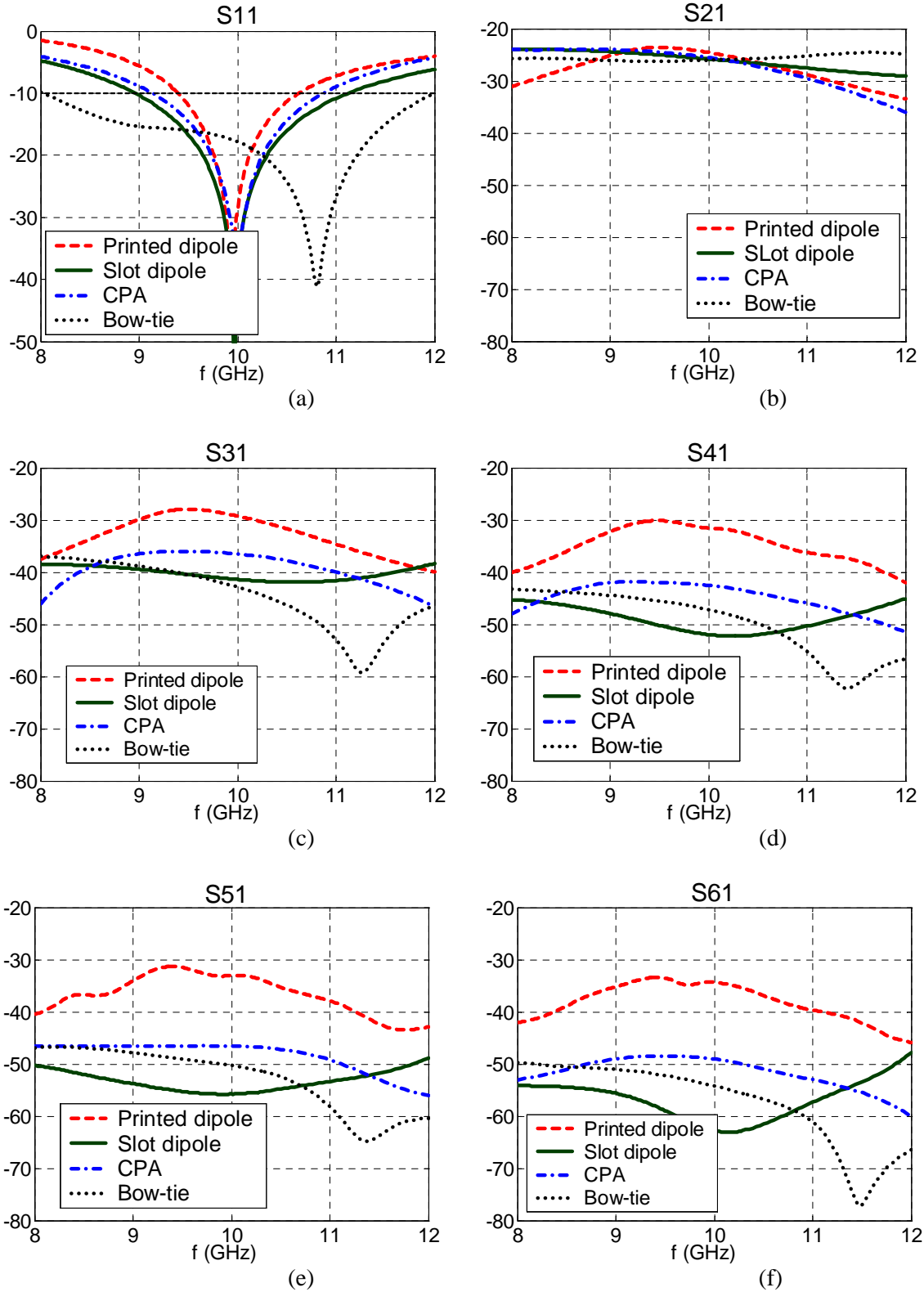


Fig. 20. Return loss and coupling between elements of 6-element array module for printed dipole, slot dipole, CPA and bow-tie slot antenna with distance between elements equals to 20.8, 3, 8.5, and 4 mm, respectively. (a) S₁₁, (b) S₂₁, (c) S₃₁ (d) S₄₁, (e) S₅₁ and (f) S₆₁.

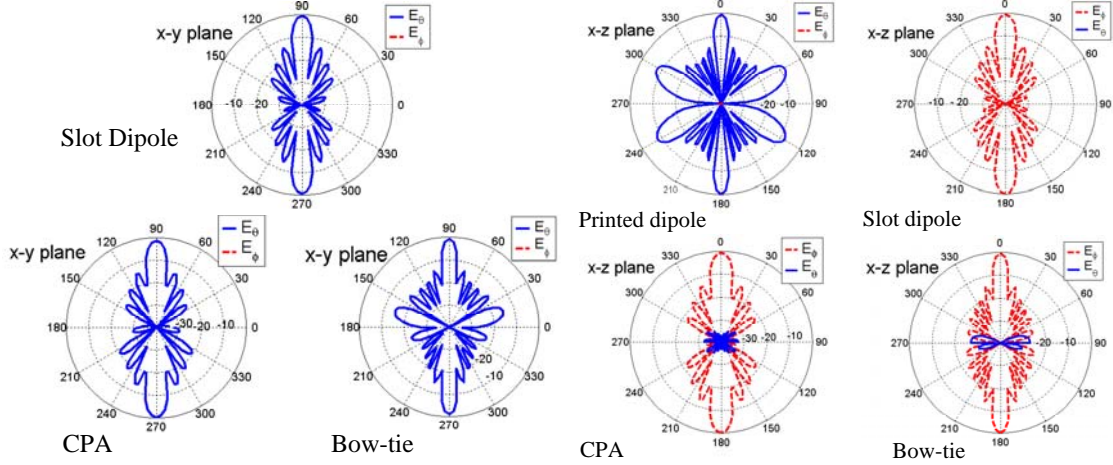


Fig. 21. Radiation pattern in x-y plane.

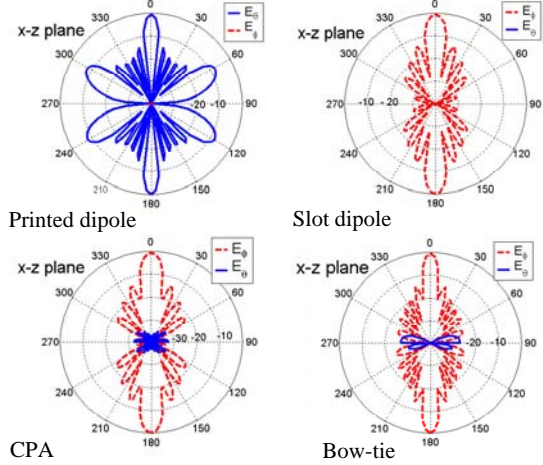


Fig. 22. Radiation pattern in x-z and y-z planes.

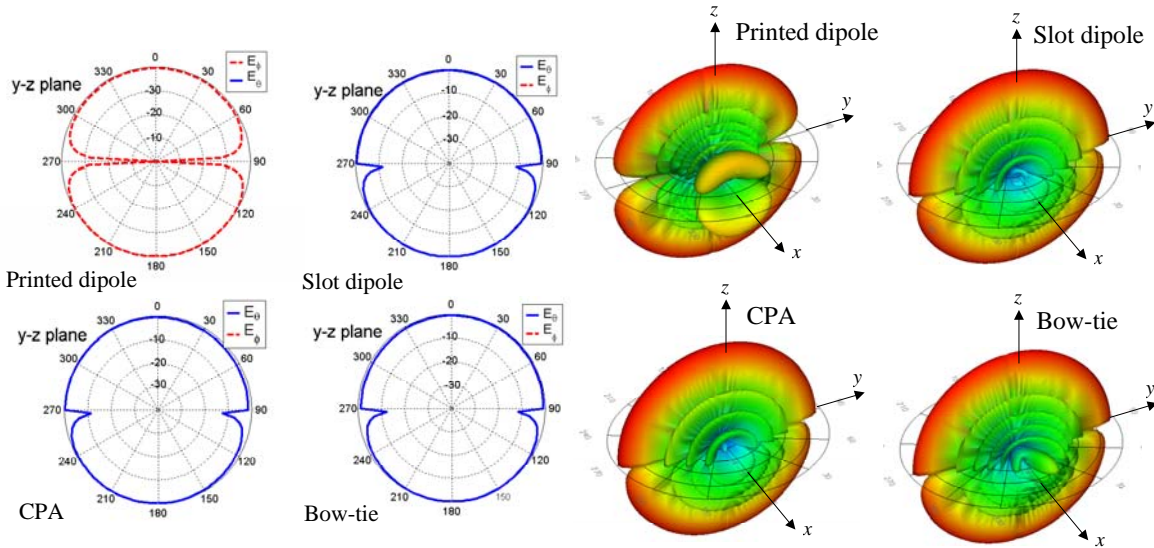


Fig. 23. Radiation pattern in x-z and y-z planes.

Fig. 24. Total 3D radiation pattern.

V. CONCLUSIONS

In this paper, a printed dipole antenna and three microstrip slot antennas operating at 10 GHz in the X-band (8-12 GHz) are presented. Parametric studies for each antenna showing the effect of each geometrical parameter and antennas' dimensions in terms of λ_g are presented. Slot antennas achieve better BW that reaches 52% for the bow-tie slot antenna. In addition, the arrays of slot antennas are smaller and have less than -24 dB coupling between elements as obtained for the 6-element arrays. The efficiencies of the slot antennas are near 80%, slightly less than the printed dipole antenna. The cross-polarization level is less than -27 dB in the x-z plane and -40 dB in the y-z plane. All antennas show good radiation pattern stability over the entire band of operation.

REFERENCES

- [1] K-L. Wong, *Compact and Broadband Microstrip Antennas*, New York, NY, *John Wiley and Sons*, 2002.
- [2] K. Li, C. H. Cheng, T. Matsuni and M. Izutsu, "Coplanar patch antennas: principal, simulation and experiment," *Proc. Antennas Propagat. Soc. Int. Symp.*, Boston, MA, vol. 3, pp. 402-405, July 2001.
- [3] K. F. Tong, K. Li, T. Matsuni and M. Izutsu, "Wideband coplanar waveguide fed coplanar patch antenna," *Proc. Antennas Propagat. Soc. Int. Symp.*, Boston, MA, vol. 3, pp. 406-409, July 2001.
- [4] A. Z. Elsherbeni, Abdelnasser A. Eldek, B. N. Baker, C. E. Smith and K-F Lee, "Wideband coplanar patch-slot antennas for radar applications," *Proc. Antennas Propagat. Soc. Int. Symp.*, Houston, TX, vol. 2, pp. 436-439, June 2002.
- [5] Yu-De Lin and Syh-Nan Tsai, "Coplanar waveguide-fed uniplanar bow-tie antenna," *IEEE Trans. Ant. Prop.*, vol. AP-45, no. 2, pp. 305-306, Feb. 2000.
- [6] A. A. Eldek, A. Z. Elsherbeni, C. E. Smith and K-F Lee, "Wideband slot antennas for radar applications," *Proc. IEEE Radar Conf.*, Huntsville, AL, pp. 79-84, May 2003.
- [7] E. A. Soliman, S. Berbels, P. Delmotte, G. A. E. Vandenbosch, and E. Beyne, "Bow-tie slot antenna fed by CPW," *Electron Lett.*, vol. 35, pp. 514-515, 1999.
- [8] Jen-Fen Huang, Chih-Wen Kuo, "CPW-fed bow-tie slot antenna," *Microwave Opt. Technol. Lett.*, vol. 19, no. 5, pp. 358-360, Dec. 1998.
- [9] M. Miao, B. L. Ooi, P. S. Kooi, "Broadband CPW-fed wide slot antenna," *Microwave Opt. Technol. Lett.*, vol. 25, no. 3, pp. 206-211, May 2000.
- [10] A. A. Eldek, A. Z. Elsherbeni and C. E. Smith, "Wideband bow-tie slot antennas for radar applications," *2003 IEEE Topical Conference on Wireless Communication Technology*, Honolulu, Hawaii, October 2003.